Nanoscale Charge-Balancing Mechanism in Alkali-Substituted Calcium−Silicate−Hydrate Gels

V. Ongun Özçelik*[,†,‡] and Claire E. White*[,†,‡]

[†]Andlinger Center for Energy and the Environment, and [‡]Department of Civil and Environmental Engineering, Princeton University, Princeton, New Jersey 08544, United States

S Supporting Information

ABSTRACT: Alkali-activated materials and related alternative cementitious systems are sustainable technologies that have the potential to substantially lower the CO_2 emissions associated with the construction industry. However, these systems have augmented chemical compositions as compared to ordinary Portland cement (OPC), which may impact the evolution of the hydrate phases. In particular, calcium-silicate-hydrate (C−S−H) gel, the main hydrate phase in OPC, is likely to be altered at the atomic scale due to changes in the bulk chemical composition, specifically via the addition of alkalis (i.e., Na or K) and aluminum. Here, via density functional theory calculations, we reveal the presence of a charge balancing mechanism at the molecular level in C−S−H gel (as modeled using crystalline 14 Å tobermorite) when alkalis and aluminum atoms are introduced into the structure. Different structural representations are obtained depending on the level of substitution and the degree of charge balancing incorporated in the structures. The impact of these substitutional and charge balancing effects on the structures is assessed by analyzing the formation energies, local bonding environments, diffusion barriers and mechanical properties. The results of this computational study provide information on the phase stability of alkali/aluminum containing C−S−H gels, shedding light on the fundamental atomic level mechanisms that play a crucial role in these complex disordered materials.
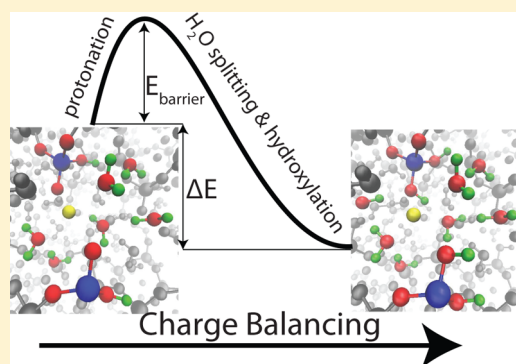
Studies in materials science have focused on developing new technologies that lower CO_2 emissions associated with the transportation, energy, and construction industries due to the emerging issues associated with climate change. For this purpose, efforts have been devoted to modify, functionalize, or replace conventional materials with their sustainable counterparts. Ordinary Portland cement (OPC) concrete is a material that has been used for centuries in construction applications ranging from bridge decks to nuclear waste encapsulation. The production of OPC clinker (an ingredient required to make OPC concrete) creates approximately 8% of human-made CO_2 emissions, and the overall quantity of CO_2 emissions from cement production is estimated to grow rapidly in coming years.[1,2] Recently, alkali-activated materials (AAMs), have been proposed as an alternative to conventional OPC, especially since AAMs reduce CO_2 emissions by up to 80%.[3−5] Moreover, depending on the type of precursor and activator used to make this material, the fundamental phase that controls the material's performance possesses similarities to the main hydration phase in OPC-based systems.

Despite the extensive history of OPC concrete usage throughout the world, there are still ambiguities regarding the atomic structure of its most critical phase, calcium-silicate-hydrate (C−S−H) gel, which is responsible in part for the strength and durability of cement paste.[6−9] Calcium-rich AAMs obtained via the alkali activation process further increase the complexity of the atomic arrangements in C−S−H gels because

of the increased chemical and physical heterogeneity of the precursor (e.g., ground granulated blast-furnace slag). Experimental studies show that the inclusion of alkali atoms (Na/K) and Al in the C−S−H gel (forming C−N−A−S−H gel, where N represents the alkali and aluminum is shown by A) has critical effects on the physical and chemical properties of the gel structure, such as increasing the OH^- concentration, changing the H_2O content, and causing a decrease in both the basal spacing of the unit-cell and the silica mean chain length.[10−12] It is generally accepted that the inclusion of alkali atoms alters the local bonding environment of C−S−H gels and requires the inclusion of hydrogen atoms to maintain charge neutrality;[13−16] however, a comprehensive understanding of the atomistic structures and the thermodynamics of the charge balancing mechanism existing in these new materials are missing, particularly with respect to the impact of alkali atoms on the relative stability of the C−S−H-like phases.

In this Letter, we present a fundamental charge balancing mechanism that influences the formation energies of a range of atomic structures representative of those found in OPC and AAM systems. Briefly, this charge balancing is initiated by the diffusion of H atoms to specific sites within the crystal structure

of 14 Å tobermorite (representative of C−S−H gel) in order to counter balance the water deprotonation that occurs as a result of substituting the interlayer Ca atoms with alkali atoms. The additional H atoms modify the chemical bonds of the structure and initiate chain reactions within the unit-cell, which leads to new structural forms of the model phases. These new phases show similar structural stabilities and bond strengths at the molecular level compared to C−S−H gel. Depending on the concentration and type of alkali atoms used, the intermolecular bonding strength, bulk modulus, unit-cell volume, and water content of the alkali containing C−S−H phase can be modified. Additionally, substituting one of the bridging Si atoms with an Al atom creates C−A−S−H gel,[17] which is the main binding phase in blended OPC pastes synthesized using aluminate-rich supplementary cementitious materials, such as fly ash and metakaolin. The atomic arrangements of C−A−S−H gel are also modified with the same charge balancing mechanism, resulting in structures with higher levels of phase stability. By combining the effects of both alkali and Al substitution, the impact of the charge balancing mechanism on the phase stability of the C−N−A−S−H gel in AAMs is assessed. Given that AAMs are crucial materials for reducing human-made CO_2 emissions associated with cement production, we believe that (i) the fundamental charge balancing mechanism proposed in this Letter, (ii) the atomistic properties associated with this mechanism, and (iii) the new model structures presented here will pave the way to a deeper understanding of the impact of alkali activation on the resulting gel phase and enhance the uptake of environmentally friendly construction materials.

Although there are numerous studies on the atomic structures of C−S−H gel and tobermorite minerals,[8,9,18−22] a model derived purely from first-principles calculations without any empirical inputs is crucial in order to obtain fundamental properties such as ground state energy, internal pressure, forces on atoms, local bonding environments and distribution of local charge between the atoms. Previous studies have shown that first-principles calculations are able to predict these fundamental properties in similar materials to a high level of accuracy.[23−29] Here, we focus on 14 Å tobermorite since this crystal structure has been used to describe C−S−H gels with Ca/Si ratio less than 1.4 and slag-based AAMs (containing C−N−A−S−H gel) tend to have a Ca/(Si+Al) ratio of 1.[30−32] After optimizing (i) the shape of the crystal unit-cell, (ii) the bond lengths, (iii) the orientation of H_2O molecules with respect to silica chains and (iv) the interlayer spacing, we end up with the optimum ground state of 14 Å tobermorite with the chemical formula of $Ca_5Si_6O_{16}(OH)_2 \cdot 7H_2O$ as presented in Figure 1. Using this optimized pure structure, we produce representative alkali containing phases by introducing alkali (Na, K) or alkali-earth (Mg) atoms to the C−S−H unit-cell via substitution with the interlayer Ca atoms. (Note that Mg is included in this study for completeness since a small amount of Mg can be found in slag. Also note that different substitution sites for the alkali atom were tested, and it was found that replacing the Ca atom in the interlayer region by an alkali atom is energetically the most favorable case.) After each substitution, we repeat the same rigorous optimization procedure as carried out for the pure case. Thus, we end up with a set of structures produced using the same theoretical approach, which is necessary for making appropriate comparisons of stability, energetics, and mechanical strength.

From the set of structures produced using the method outlined above, it is seen that once a Ca atom is replaced by an
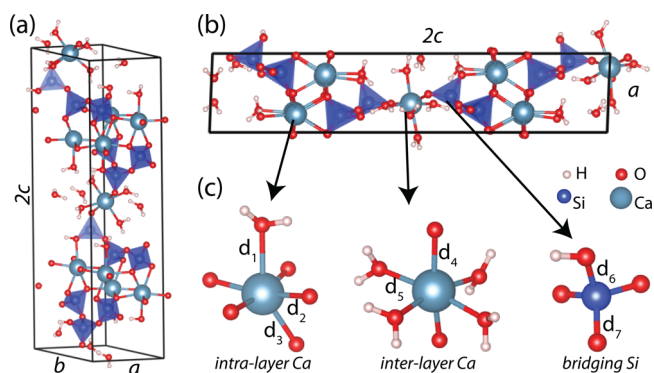

Figure 1. Model C−S−H structure represented by 14 Å tobermorite in (a) perspective and (b) side view. (c) Bonding geometries of intralayer Ca, interlayer Ca, and bridging Si. O, H, Si, and Ca atoms are shown with red, white, blue, and light blue spheres, respectively, using a ball-and-stick model. Selected bond lengths and unit-cell dimensions are indicated where $d_1 = 2.57$ Å, $d_2 = 2.38$ Å, $d_3 = 2.42$ Å, $d_4 = 2.30$ Å, $d_5 = 2.45$ Å, $d_6 = 1.67$ Å, $d_7 = 1.60$ Å, $a = 6.57$ Å, $b = 7.36$ Å, and $2c = 28.01$ Å. It should be noted that the interlayer Ca atom is in 6-fold coordination, with the seventh O atom belonging to a water molecule having a Ca−O distance of 3.41 Å.

alkali atom, the charge neutrality of the structure is broken in the vicinity of the substitution site, due to the fact that we are effectively removing a $^{+2}$ ion (Ca^{2+}) and replacing it with a $^{+1}$ ion (Na^+ or K^+). Thus, the crystal is deprotonated by creating a hole in its electronic structure, which is a potential source of local instability under an external stimulus or in the presence of a foreign chemical agent. Since our prime objective is to maintain structural and chemical stability of the material, we counter balance this deprotonation by introducing an external H atom and reoptimizing the atomic positions in the unit-cell to obtain a charge balanced C−S−H[N,n] or C−A−S−H[N,n] structure where N represents the atom that substitutes the interlayer Ca atom and n is the number of H atoms used for charge balancing. In addition to the need to charge balance the structure due to alkali substitution, it is also necessary to perform the same procedure when a bridging silicon is replaced by aluminum, as is evident in the results in this Letter. It should be noted that the addition of an extra H atom to the system is representative of the charge balancing mechanism that occurs during the alkali activation process when Na/K is included in the C−S−H and/or C−A−S−H gel. However, during formation of these gels, there is an abundance of ions in the solution, including a significant amount of OH− groups due to the high pH environment. Hence, it is likely that these OH− groups that are present during formation of the material serve the same purpose as the H atom introduced in our DFT calculations, leading to a gel structure that contains a higher amount of chemically bound OH^- groups when alkalis and aluminum are incorporated into the structure. Nevertheless, using these DFT calculations, we are able to unravel the impact of the individual chemical steps involved in the charge balancing mechanism at the atomic level.

The variation in the total energy during structural optimization is a powerful tool for investigating the development of new chemical interactions that may emerge during the structural rearrangements of atoms. It also provides information on any transient phases present during the optimization process together with the possible energy barriers that need to be overcome for the structure to reach its ground state.[33−38]

Therefore, to investigate the atomic self-rearrangements taking place during charge balancing, we performed a systematic analysis of the charge balancing process in the alkali containing C−S−H gel structure, taking into account all intermediate steps. Specifically, after substitution of an interlayer Ca atom for an alkali atom and insertion of a H atom, we compared the ground state energies of various bonding sites in the structure for the extra H atom and found the optimal position (lowest ground state). Using the initial structure (containing the alkali and a H atom) and the final optimum structure, we determined the intermediate steps leading to this optimum structure using self-consistent conjugate gradient calculations. During the simulation of the intermediate steps, both the atom positions and the lattice constants were optimized at each step to capture the dynamics of the atomic rearrangements.

Figure 2 shows the variation of the total energy of the C−S−H[Na,H] unit-cell during the charge balancing process together
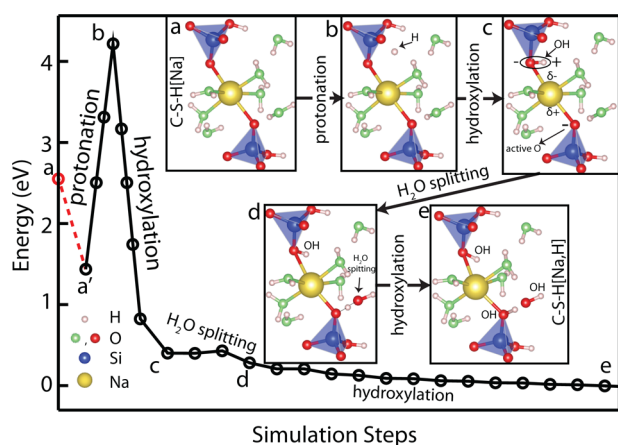

Figure 2. Variation of total energy during the charge balancing process of the C−S−H model structure (based on 14 Å tobermorite) where the energy of the optimized charge balanced structure is taken as zero. The insets (a−e) show the self-rearrangements of atoms during charge balancing. (a) Optimized structure of Na-doped C−S−H[Na]. (b) Protonation of the unit-cell as the H atom moves into the interlayer region. (c) OH formation and charge induction on the alkali atom. (d) Charge balancing via dissociation of H_2O. (e) Formation of additional OH. In the energy curve, point a′ shows the total total energy of (C−S−H[Na] + isolated H atom) system and the total energy of C−S−H[Na] is shown by a. In the ball-and-stick model, oxygen atoms in H_2O and OH are shown with green and red spheres, respectively.

with the structural self-rearrangements of the atoms. It is clear in this figure that there are three fundamental steps (protonation by the addition of H atom, H_2O splitting, and hydroxylation), all of which contribute to the formation of a symmetrical charge distribution around the alkali atom. At the beginning of the charge balancing process, the structure consists of the optimized charge unbalanced C−S−H[Na] phase and a H atom randomly inserted in the interlayer region (illustrated in insets a and b of Figure 2). Due to the random initial location of the H atom, the total energy of the system suddenly increases by 2.8 eV (to state b in Figure 2). Hence, this is the energy barrier that the H atom needs to overcome to reach its most favorable location, which is near the O atom situated between the bridging silica site and the alkali atom (inset c of Figure 2). Eventually, the H atom forms an OH bond at one end of the alkali atom and the total energy of the unit-cell drops by 3.8 eV from point b to c. The newly created

OH dipole momentarily polarizes the alkali atom, which then induces a negative charge of 0.8e on the O atom located on the opposite side of the alkali atom. Thus, the O atom between the lower bridging silica site and the alkali atom becomes chemically active. Due to its increased chemical activity, the free H_2O molecule in the interlayer region is attracted to this O atom, (as shown by inset d of Figure 2). Eventually, H_2O dissociates into a H^+ and OH^- ion, and the H^+ ion establishes another OH bond near the lower bridging silicon site as shown in inset e. As a result of this sequence of chemical reactions, the addition of the initial H atom leads to the formation of three extra OH groups along with the dissociation of one H_2O molecule. It should be noted that during this process the other H_2O molecules bonded to the alkali atom rotate to maintain a symmetrical charge distribution. Overall, as a result of the charge balancing steps, the total energy of the unit-cell drops by 1.4 eV, resulting in a more stable structure. The same charge balancing steps are also observed when the unit-cell contains K instead of Na.

An important consideration for OPC concrete containing Al-rich supplementary cementitious materials (such as fly ash and metakaolin) and Ca-rich AAM phases (which also contain a sizable amount of Al) is the impact of Al on the energetics and mechanical properties of the resulting binding gel. In Ca-rich AAMs, these alkali containing gels, known as C−N−A−S−H gels, are obtained by substituting a Si atom with an Al atom as well as replacing an interlayer Ca with an alkali atom. Thus, effectively 2 protons are removed from the vicinity of the substitution site, which necessitates the addition of 2 protons to the unit-cell for proper charge balancing and chemical stability. The mechanism proposed above for the alkali containing C−S−H gel is also valid for C−N−A−S−H. Here, replacing the bridging Si with Al causes this site to become negatively charged (due to the loss of a proton), which induces a negative charge on the neighboring O atom, as illustrated in Figure 3a,b. The negatively charged O atom attracts the nearby H_2O molecule and subsequently dissociates it into a OH^- and H^+ ion. This H^+ ion forms an OH group on the bridging site. Thus, when Si is replaced with Al, initially the unit-cell dehydrates by
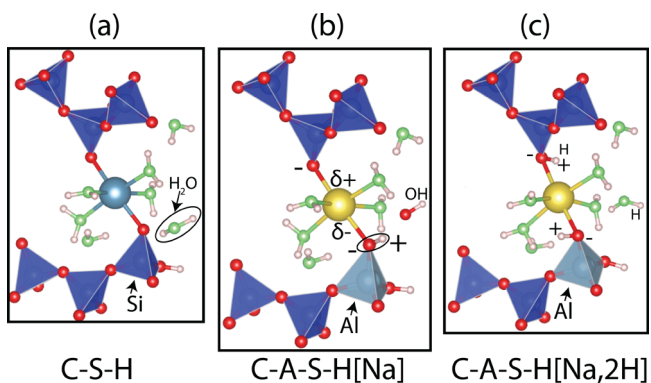

Figure 3. Formation of charge-balanced C−A−S−H[Na,2H] from C−S−H. (a) Initial C−S−H structure. (b) Charge unbalanced C−A−S−H structure after the substitution of the interlayer Ca with Na and the bridging Si with Al. One water molecule is dissociated, and two OH molecules are created, which hydroxylate the interlayer region. In the final structure, there are six water molecules around the Na atom. (c) Charge balance is reobtained by the addition of two external H atoms. The final structure has the same water content as the initial C−S−H structure, while the interlayer region is hydroxylated.

one water molecule and two new OH groups are created in the interlayer region (one OH is bonded to Al and the other one is free). The OH group, which is bonded to Al, triggers a charge induction chain reaction in a similar manner to the one explained in the previous paragraph. As shown in Figure 3c, the first externally added H atom attaches to the O atom that is at the other end of the alkali atom (and associated with the silica bridging site). The second H atom added to the system neutralizes the free OH ion present in the interlayer, reestablishing the H_2O molecule that disassociated in the previous step. In the end, we acquire a charge balanced alkali containing C−A−S−H gel, (i.e., C−A−S−H[Na,2H]), that preserves the initial water content and is chemically stable. Interestingly, this process causes the protonation of the bridging sites in the (alumino)silicate chains by two new OH groups per unit-cell, which requires experimental verification. It should also be noted that the incorporation of an alkali within the C−A−S−H structure reduces the unit-cell volume and basal spacing by 0.5%.

The thermodynamic stabilities of the charge balanced structures discussed so far can be evaluated by comparing their cohesive energies. The cohesive energy per unit-cell is defined as $E_c = \sum_i n_i E_i - E_{structure}$,[39] and therefore it is the difference between the sum of energies of the free atoms present in the unit-cell and the total energy of the overall structure in its optimized geometry. Here, n_i is the number of i atoms present in the unit-cell and E_i is the ground state energy of the ith atom. It should be noted that the single atom energies were calculated taking into account their magnetic ground states according to Lieb's theorem.[40] (This analysis was carried out for each isolated atom to obtain the following magnetic ground states: H: 1 μ_B, Ca: 0 μ_B, Al: 1 μ_B, K: 1 μ_B, Mg: 0 μ_B, Na: 1 μ_B, O: 2 μ_B and Si: 2 μ_B.) E_c by itself signifies the energy gained per unit-cell by constructing a particular phase from its constituent atoms. Due to the strong covalent and ionic bonds present in these gels, all of them have high cohesive energies, indicating stability at ambient conditions. However, for practical purposes and bench marking, we need to determine the formation energies of these phases with respect to the well-known C−S−H gel. The formation energy is the difference between the cohesive energies, $E_f[X] = E_c[X] - E_c[C-S-H]$, where X is phase of interest and $E_c[C-S-H]$ is the cohesive energy of 14 Å tobermorite that is used to represent C−S−H gel in this study. We use these E_f values as the primary criterion for determining whether an energy loss or gain is associated with the substitution of each alkali/aluminum atom, where a negative E_f value implies a less favorable structure compared with C−S−H gel.

As shown in Figure 4a, substitution of the interlayer Ca with Na (or K) leads to an energy loss of 5.5 eV (or 6.3 eV). The cost of K doping is slightly higher than Na doping, which is a result of the larger atomic radius of K causing a greater distortion to the unit-cell. In a similar fashion, NaAl doped C−S−H gel (or C−A−S−H[Na]) is also less favorable than the initial C−S−H gel by 9.1 eV. After the charge balancing process, the energy loss associated with the Na and K doped structures, namely, C−S−H[Na,H] and C−S−H[K,H], reduce to 0.4 and 1.1 eV, respectively. Remarkably, the C−A−S−H[Na,2H] structure, which forms after charge balancing of the Na doped C−A−S−H gel, is more favorable than the initial pure C−S−H gel by 0.95 eV. Apart from improving the stability of the alkali containing gels, charge balancing also creates more compact and tightly bound crystal structures, as
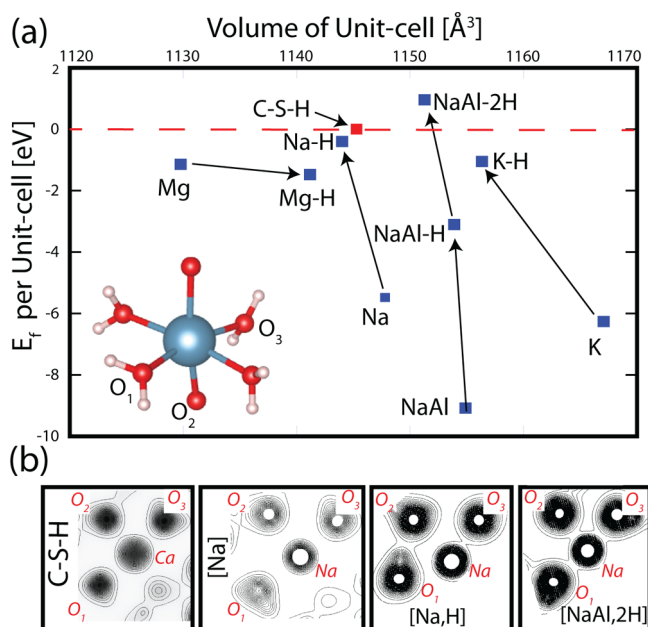

Figure 4. (a) Formation energies of Na, K, Mg, NaAl-doped C−S−H gel, and their charge balanced structures (indicated with H or 2H) with respect to the pure C−S−H structure. The cohesive energy of pure C−S−H is taken as zero. Negative formation energies correspond to less favorable structures as compared with C−S−H. We note that NaAl indicates the structure that forms after the substitution of Ca by Na and bridging Si by Al. (b) Charge density contour plots on the plane passing from the interlayer atom and its neighboring O atoms. We also note that bond strength increases as H atoms are introduced for charge balancing. Atomic configurations of the structures are provided as Supporting Information.

evidenced by the reduction of the crystal unit-cell volume by up to 2%. It should be noted that, as opposed to alkali substitution, Mg substitution creates a smaller energy loss of only 1.1 eV due to the fact that Mg also has a + 2 ionic configuration. As expected according to charge balancing arguments, the C−S−H[Mg,H] structure is a positively charged model that is less favorable than the initial C−S−H[Mg] structure (by 0.15 eV). Furthermore, the introduction of a H atom in the C−S−H[Mg] structure leads to a 1.4% increase in the unit-cell volume. Hence, it is clear that changes in the formation energy and unit-cell volume can both be used to assess the impact of alkalis and aluminum on the stability of C−S−H gel.

The improved stability of the crystals after charge balancing is also apparent in their local charge densities. In Figure 4b, we present charge density contour plots for the C−S−H, C−S−H[Na], C−S−H[Na,H], and C−A−S−H[Na,2H] structures, calculated on the plane passing through the interlayer Ca/Na site and O atoms (as depicted in Figure 4a). In each calculation, the contour interval is chosen to be the same (0.1 eV/A^2) and a denser grid implies stronger bonding. It is seen that the interlayer Ca atom has stronger bonds with its neighboring O atoms in C−S−H gel compared with the weaker bonding involving the interlayer Na atom in C−S−H[Na]. However, these weak bonds regain strength upon proper charge balancing of the unit-cell, and eventually the C−A−S−H[Na,2H] gel has the strongest local bonds around the interlayer atom. Hence, these results on the bond strength in the structures provide further evidence that charge balancing of the alkali containing structures via addition of H atoms leads to phases that are

chemically more stable than their charge unbalanced counterparts.

We finally turn our attention to the effects of charge balancing on the macroscopic observable signatures of stability such as the bulk modulus and the diffusion barriers of atoms within the unit-cell. The bulk modulus of a crystal can be obtained using the equation $K = -V^{opt}dP/dV = -V^{opt} d^2E/dV^2$, where the second derivative of the total energy (E) with respect to unit-cell volume (V) is calculated in the vicinity of V^{opt} (volume corresponding to the energetically most favorable configuration), within the harmonic approximation. While calculating the energies in the vicinity of V^{opt}, the volume of the unit-cell was uniformly changed within the range of $\pm 3\%$ of V^{opt} and the atomic positions within the unit-cell were reoptimized for each volume. Using this approach, the bulk modulus of 14 Å tobermorite (representing C−S−H gel) is calculated to be 54 GPa, and is seen to reduce to 49 GPa for C−S−H[Na] (36 GPa for C−S−H[K]). After charge balancing, this value increases to 52 GPa for C−S−H[Na,H] (40 GPa for C−S−H[K,H]), which further increases to 66 GPa for the charge-balanced C−A−S−H[Na,2H] gel. These calculated bulk modulus values are in agreement with the experimentally obtained value of 47 GPa for 14 Å tobermorite[41] and other computational studies that use ab initio and force field methods.[16,42−46] It is important to note that the structure representative of C−N−A−S−H gel in AAMs (C−A−S−H[Na,2H]) has the highest bulk modulus value, and this information combined with the formation energy results and bond strength data provides evidence that these alternative cements may be as stable as the C−S−H gel in OPC paste. This is consistent with a previous study, which reported an increase in the bulk modulus value as the Ca/Si ratio is lowered.[16] However, additional research is required to fully determine the degree of stability of the gel phases in AAMs and OPC, including the impact of nanoscale disorder (i.e., nanocrystalline versus amorphous)[47] and local defects (e.g., finite silica chain lengths).

For materials where the atoms can move from a well-defined lattice site, the bulk modulus of the structure is closely related to the activation energy associated with diffusion (or diffusion barrier) of its constituent atoms.[48] Thus, as another way of demonstrating the effect of charge balancing on mechanical strength, we finally calculate the diffusion barrier of the interlayer Na atom in the model structure of C−S−H[Na] gel and compare it with the mobility of the Na atom in the charge balanced C−S−H[Na,H] gel structure. The minimum diffusion barriers have been obtained by analyzing the energy landscapes of the Na atom in the interlayer region, which are shown in Figure 5. The energy landscape of each structure was calculated by manually placing the Na atom at various positions in the interlayer region and performing self-consistent geometry optimization for the surrounding atoms. During this geometry optimization, the Na atom is kept fixed at a particular position on the horizontal xy plane while its z coordinate is relaxed, which allows us to scan a 3D energy path for the interlayer atom. This calculation was repeated to obtain the ground state energies for a total of 100 points that were uniformly distributed on the xy-plane of the unit-cell and the energy values of the remaining points were determined by interpolation of the calculated data. Thus, possible migration paths for the Na atom, which align with the minimum diffusion barriers, are obtained as indicated by the white stars in Figure 5. It is seen that the Na atom needs to overcome a barrier of 1.18
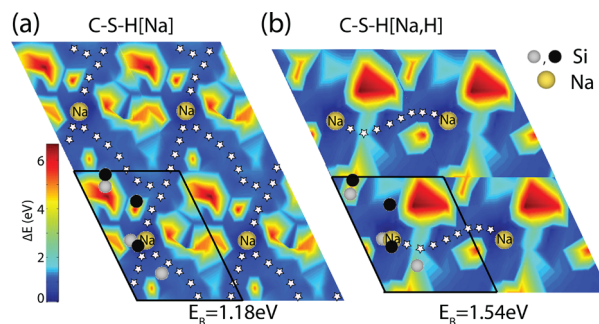

Figure 5. (a) Energy landscape for the Na atom in the interlayer region of C−S−H[Na] plotted on the 2 × 2 unit-cell. Its migration path along the minimum energy barrier is indicated by white stars. (b) Energy landscape for the charge balanced C−S−H[Na,H]. Note that, upon charge balancing, the activation energy for diffusion increases from 1.18 to 1.54 eV, which is an indication of increased mechanical strength. In the energy landscapes, blue regions represent more favorable sites for the Na atom as compared with red regions. The Si atoms below and above the Na atom in the interlayer region are represented by gray and black spheres respectively, and the diffusing Na atom is represented by a yellow sphere.

eV in the C−S−H[Na] structure, whereas this barrier increases to 1.54 eV for the charge balanced C−S−H[Na,H] structure. The increase in the diffusion barrier upon charge balancing provides further evidence of improved structural stability via the symmetrical charge balancing mechanism proposed in this Letter. It should also be noted that the diffusion barrier for the Ca atom in pure C−S−H was calculated to be 1.61 eV, and therefore the migration barrier trends according to alkali substitution and charge balancing are consistent with the bulk modulus and formation energy trends for these structures.

In conclusion, the proposed charge balancing mechanism outlined in this Letter sheds light on the fundamental atomic structural arrangements existing in cement-based gels that contribute to the macroscopically measured properties. We show that the charge balancing process, which consists of protonation, hydroxylation, and water dissociation steps, is a dominant factor governing the ground state structures of the atomistic models representative of these low-CO_2 materials. The inclusion of Na (or K) in the gel can lead to a highly stable phase, but only if the alkali is accompanied by a bridging Al site and the proper amount of H atoms for charge balancing. These models imply that the long-term phase stability and mechanical strength of Ca-rich AAMs are in the same range of C−S−H-based OPC systems, provided that proper charge balancing takes place during their synthesis. However, further research is required to assess the impact of nanoscale structural disorder on phase stability, which may be an important aspect governing the mechanical and physical properties of these alkali-activated gels.

■ METHODS

Our predictions were obtained from state-of-the-art first-principles pseudopotential calculations based on the spin-polarized DFT within the generalized gradient approximation (GGA) including van der Waals corrections.[49] The optimized structures, total energy calculations, diffusion barrier results, and bulk modulus values presented in this Letter were obtained from numerical calculations that were carried out using the VASP software.[50] During these calculations, we used projector-augmented wave potentials (PAW),[51] and the exchange-

correlation potential has been approximated with the Perdew–Burke–Ernzerhof (PBE) functional.[52] The Brillouin zone (BZ) was sampled in the Monkhorst–Pack scheme, where the convergence in energy as a function of the number of **k**-points was tested. The **k**-point sampling of $(3 \times 3 \times 3)$ was found to be suitable for the BZ corresponding to the primitive unit-cell of 14 Å tobermorite. The same **k**-point sampling was used for each of the alkali containing structures. During structure optimization calculations, the atomic positions were optimized using the conjugate gradient method, where the total energy and atomic forces were minimized and the lattice constants were optimized for each structure. The energy convergence value between two consecutive steps was chosen as 10^{-5} eV, resulting in a maximum force of 0.1 eV/Å on each atom. In charge transfer calculations, Mulliken charges are preferred because we are interested in the charge of the atoms calculated by atomic orbitals rather than obtaining atomic charges based on plane wave electron density calculations as implemented in VASP. Mulliken charge densities were calculated using the SIESTA code[53] starting from the preconverged structures obtained in VASP. A 200 Ryd mesh cutoff was chosen, and the self-consistent field (SCF) calculations were performed with a mixing rate of 0.1. Core electrons were replaced by norm-conserving, nonlocal Troullier–Martins pseudopotentials.[54] In the Mulliken charge calculations, the exchange-correlation potential was approximated by GGA using the PBE functional.[52] We finally note that all of the computations were performed using a $1 \times 1 \times 2$ unit-cell (with dimensions a, b, and $2c$) in order to account for the partial occupancies of the one Ca atom and three H_2O molecules that are present in the atomic structure files available in the literature.

■ ASSOCIATED CONTENT

Ⓢ Supporting Information

The Supporting Information is available free of charge on the ACS Publications website at DOI: 10.1021/acs.jpclett.6b02233.

Atomic configurations of the structures (ZIP)

■ AUTHOR INFORMATION

Corresponding Authors
*E-mail: ongun@princeton.edu.
*E-mail: whitece@princeton.edu.

ORCID Ⓞ
V. Ongun Özçelik: 0000-0003-0645-7231

Notes
The authors declare no competing financial interest.

■ ACKNOWLEDGMENTS

■ REFERENCES

(1) Scrivener, K. L.; Kirkpatrick, R. J. Innovation in Use and Research on Cementitious Material. *Cem. Concr. Res.* **2008**, *38*, 128−136.

(2) Van Ruijven, B. J.; Van Vuuren, D. P.; Boskaljon, W.; Neelis, M. L.; Saygin, D.; Patel, M. K. Long-term Model-based Projections of Energy Use and CO_2 Emissions from the Global Steel and Cement Industries. *Resour. Conserv. Recy.* **2016**, *112*, 15−36.

(3) Duxson, P.; Provis, J. L.; Lukey, G. C.; van Deventer, J. S. J. The Role of Inorganic Polymer Technology in the Development of Green Concrete. *Cem. Concr. Res.* **2007**, *37*, 1590−1597.

(4) McLellan, B. C.; Williams, R. P.; Lay, J.; van Riessen, A.; Corder, G. D. Costs and Carbon Emissions for Geopolymer Pastes in Comparison to Ordinary Portland Cement. *J. Cleaner Prod.* **2011**, *19*, 1080−1090.

(5) Myers, R. J.; Bernal, S. A.; San Nicolas, R.; Provis, J. L. Generalized Structural Description of Calcium-sodium Aluminosilicate Hydrate Gels: The Cross-linked Substituted Tobermorite Model. *Langmuir* **2013**, *29*, 5294−5306.

(6) Allen, A. J.; Thomas, J. J.; Jennings, H. M. Composition and Density of Nanoscale Calcium-Silicate-Hydrate in Cement. *Nat. Mater.* **2007**, *6*, 311−316.

(7) Richardson, I. G. The Nature of CSH in Hardened Cements. *Cem. Concr. Res.* **1999**, *29*, 1131−1147.

(8) Abdolhosseini Qomi, M. J.; Krakowiak, K. J.; Bauchy, M.; Stewart, K. L.; Shahsavari, R.; Jagannathan, D.; Brommer, D. B.; Baronnet, A.; Buehler, M. J.; Yip, S.; et al. Combinatorial Molecular Optimization of Cement Hydrates. *Nat. Commun.* **2014**, *5*, 4960.

(9) Skinner, L. B.; Chae, S. R.; Benmore, C. J.; Wenk, H. R.; Monteiro, P. J. M. Nanostructure of Calcium Silicate Hydrates in Cements. *Phys. Rev. Lett.* **2010**, *104*, 195502.

(10) L'Hôpital, E.; Lothenbach, B.; Scrivener, K.; Kulik, D. A. Alkali Uptake in Calcium Alumina Silicate Hydrate (CASH). *Cem. Concr. Res.* **2016**, *85*, 122−136.

(11) L'Hôpital, E.; Lothenbach, B.; Kulik, D. A.; Scrivener, K. Influence of Calcium to Silica Ratio on Aluminium Uptake in Calcium Silicate Hydrate. *Cem. Concr. Res.* **2016**, *85*, 111−121.

(12) Faucon, P.; Delagrave, A.; Petit, J. C.; Richet, C.; Marchand, J. M.; Zanni, H. Aluminum Incorporation in Calcium Silicate Hydrates (CSH) Depending on Their Ca/Si Ratio. *J. Phys. Chem. B* **1999**, *103*, 7796−7802.

(13) Richardson, I. G. Tobermorite/jennite-and tobermorite/calcium hydroxide-based models for the structure of CSH: applicability to hardened pastes of tricalcium silicate, β-dicalcium silicate, Portland cement, and blends of Portland cement with blast-furnace slag, metakaolin, or silica fume. *Cem. Concr. Res.* **2004**, *34*, 1733−1777.

(14) Abdolhosseini Qomi, M. J.; Ulm, F.-J.; Pellenq, R. J. M. Evidence on the Dual Nature of Aluminum in the Calcium-Silicate-Hydrates Based on Atomistic Simulations. *J. Am. Ceram. Soc.* **2012**, *95*, 1128−1137.

(15) Manzano, H.; Dolado, J. S.; Griebel, M.; Hamaekers, J. A molecular dynamics study of the aluminosilicate chains structure in Al-rich calcium silicate hydrated (C-S-H) gels. *Phys. Status Solidi A* **2008**, *205*, 1324−1329.

(16) Puertas, F.; Palacios, M.; Manzano, H.; Dolado, J. S.; Rico, A.; Rodríguez, J. A model for the CASH gel formed in alkali-activated slag cements. *J. Eur. Ceram. Soc.* **2011**, *31*, 2043−2056.

(17) Skibsted, J.; Andersen, M. D. The Effect of Alkali Ions on the Incorporation of Aluminum in the Calcium Silicate Hydrate (C-S-H) Phase Resulting from Portland Cement Hydration Studied by ^{29}Si MAS NMR. *J. Am. Ceram. Soc.* **2013**, *96*, 651−656.

(18) Richardson, I. G. Model Structures for C-(A)-S-H(I). *Acta Crystallogr., Sect. B: Struct. Sci., Cryst. Eng. Mater.* **2014**, *70*, 903−923.

(19) Myers, R. J.; Bernal, S. A.; Provis, J. L. A Thermodynamic Model for C-(N-)A-S-H Gel: CNASHss. Derivation and Validation. *Cem. Concr. Res.* **2014**, *66*, 27−47.

(20) Pellenq, R. J. M.; Kushima, A.; Shahsavari, R.; Van Vliet, K. J.; Buehler, M. J.; Yip, S.; Ulm, F.-J. A Realistic Molecular Model of Cement Hydrates. *Proc. Natl. Acad. Sci. U. S. A.* **2009**, *106*, 16102−16107.

(21) Merlino, S.; Bonaccorsi, E.; Armbruster, T. The Real Structure of Tobermorite 11Å. *Eur. J. Mineral.* **2001**, *13*, 577−590.

(22) Rejmak, P.; Dolado, J. S.; Stott, M. J.; Ayuela, A. ^{29}Si Chemical Shift Anisotropies in Hydrated Calcium Silicates: A Computational Study. *J. Phys. Chem. C* **2013**, *117*, 8374−8380.

(23) Saritas, K.; Ataca, C.; Grossman, J. C. Predicting Electronic Structure in Tricalcium Silicate Phases with Impurities Using First-Principles. *J. Phys. Chem. C* **2015**, *119*, 5074−5079.

(24) Durgun, E.; Manzano, H.; Pellenq, R. J. M.; Grossman, J. C. Understanding and Controlling the Reactivity of the Calcium Silicate Phases from First Principles. *Chem. Mater.* **2012**, *24*, 1262−1267.

(25) Manzano, H.; Durgun, E.; Abdolhosseini Qomi, M. J.; Ulm, F.-J.; Pellenq, R. J. M.; Grossman, J. C. Impact of Chemical Impurities on the Crystalline Cement Clinker Phases Determined by Atomistic Simulations. *Cryst. Growth Des.* **2011**, *11*, 2964−2972.

(26) Durgun, E.; Manzano, H.; Kumar, P. V.; Grossman, J. C. The Characterization, Stability, and Reactivity of Synthetic Calcium Silicate Surfaces from First Principles. *J. Phys. Chem. C* **2014**, *118*, 15214−15219.

(27) White, C. E.; Henson, N. J.; Daemen, L. L.; Hartl, M.; Page, K. Uncovering the True Atomic Structure of Disordered Materials: The Structure of a Hydrated Amorphous Magnesium Carbonate ($MgCO_3$·3D$_2$O). *Chem. Mater.* **2014**, *26*, 2693−2702.

(28) Pegado, L.; Labbez, C.; Churakov, S. V. Mechanism of Aluminium Incorporation into C-S-H from Ab Initio Calculations. *J. Mater. Chem. A* **2014**, *2*, 3477−3483.

(29) Churakov, S. V.; Labbez, C.; Pegado, L.; Sulpizi, M. Intrinsic Acidity of Surface Sites in Calcium Silicate Hydrates and Its Implication to Their Electrokinetic Properties. *J. Phys. Chem. C* **2014**, *118*, 11752−11762.

(30) Bonaccorsi, E.; Merlino, S.; Kampf, A. R. The Crystal Structure of Tobermorite 14 Å (Plombierite), a C-S-H Phase. *J. Am. Ceram. Soc.* **2005**, *88*, 505−512.

(31) Richardson, I. G. The Importance of Proper Crystal-chemical and Geometrical Reasoning Demonstrated Using Layered Single and Double Hydroxides. *Acta Crystallogr., Sect. B: Struct. Sci., Cryst. Eng. Mater.* **2013**, *69*, 150−162.

(32) Myers, R. J.; Bernal, S. A.; Gehman, J. D.; van Deventer, J. S. J.; Provis, J. L. The Role of Al in Cross-Linking of Alkali-Activated Slag Cements. *J. Am. Ceram. Soc.* **2015**, *98*, 996−1004.

(33) Özçelik, V. O.; Durgun, E.; Ciraci, S. New Phases of Germanene. *J. Phys. Chem. Lett.* **2014**, *5*, 2694−2699.

(34) Gurel, H. H.; Özçelik, V. O.; Ciraci, S. Dissociative Adsorption of Molecules on Graphene and Silicene. *J. Phys. Chem. C* **2014**, *118*, 27574−27582.

(35) Özçelik, V. O.; Cahangirov, S.; Ciraci, S. Stable Single-layer Honeycomblike Structure of Silica. *Phys. Rev. Lett.* **2014**, *112*, 246803.

(36) Li, H.; Huang, M.; Cao, G. Markedly Different Adsorption Behaviors of Gas Molecules on Defective Monolayer MoS$_2$: A First-principles Study. *Phys. Chem. Chem. Phys.* **2016**, *18*, 15110−15117.

(37) Jiang, J.; Pachter, R.; Demeritte, T.; Ray, P. C.; Islam, A. E.; Maruyama, B.; Boeckl, J. J. Modeling Graphene with Nanoholes: Structure and Characterization by Raman Spectroscopy with Consideration for Electron Transport. *J. Phys. Chem. C* **2016**, *120*, 5371−5383.

(38) Ersan, F.; Arslanalp, Ö.; Gökoğlu, G.; Aktürk, E. Effect of Adatoms and Molecules on the Physical Properties of Platinum Doped and Substituted Silicene: A First-principles Investigation. *Appl. Surf. Sci.* **2016**, *371*, 314−321.

(39) Kittel, C. *Introduction to Solid State Physics*; John Wiley & Sons: New York, 1971.

(40) Lieb, E. H. Two Theorems on the Hubbard Model. *Phys. Rev. Lett.* **1989**, *62*, 1201−1204.

(41) Oh, J. E.; Clark, S. M.; Wenk, H.-R.; Monteiro, P. J. M. Experimental Determination of Bulk modulus of 14Å Tobermorite Using High Pressure Synchrotron X-ray Diffraction. *Cem. Concr. Res.* **2012**, *42*, 397−403.

(42) Shahsavari, R.; Buehler, M. J.; Pellenq, R. J. M.; Ulm, F.-J. First-principles Study of Elastic Constants and Interlayer Interactions of Complex Hydrated Oxides: Case Study of Tobermorite and Jennite. *J. Am. Ceram. Soc.* **2009**, *92*, 2323−2330.

(43) Manzano, H.; Dolado, J. S.; Guerrero, A.; Ayuela, A. Mechanical Properties of Crystalline Calcium-Silicate-Hydrates: Comparison with Cementitious C-S-H Gels. *Phys. Status Solidi A* **2007**, *204*, 1775−1780.

(44) Manzano, H.; Dolado, J. S.; Ayuela, A. Elastic Properties of the Main Species Present in Portland Cement Pastes. *Acta Mater.* **2009**, *57*, 1666−1674.

(45) Jackson, M. D.; Moon, J.; Gotti, E.; Taylor, R.; Chae, S. R.; Kunz, M.; Emwas, A.-H.; Meral, C.; Guttmann, P.; Levitz, P.; et al. Material and Elastic Properties of Al-tobermorite in Ancient Roman Seawater Concrete. *J. Am. Ceram. Soc.* **2013**, *96*, 2598−2606.

(46) Mejia, S.; Hoyos, B. Changes in the elastic moduli of C-S-H due to presence of interlaminar cations. *Modell. Simul. Mater. Sci. Eng.* **2016**, *24*, 035018.

(47) White, C. E.; Daemen, L. L.; Hartl, M.; Page, K. Intrinsic Differences in Atomic Ordering of Calcium (Alumino) Silicate Hydrates in Conventional and Alkali-activated Cements. *Cem. Concr. Res.* **2015**, *67*, 66−73.

(48) Wentzcovitch, R. M.; Justo, J. F.; Wu, Z.; da Silva, C. R. S.; Yuen, D. A.; Kohlstedt, D. Anomalous Compressibility of Ferroperi-clase Throughout the Iron Spin Cross-over. *Proc. Natl. Acad. Sci. U. S. A.* **2009**, *106*, 8447−8452.

(49) Grimme, S. Semiempirical GGA-Type Density Functional Constructed with a Long-Range Dispersion Correction. *J. Comput. Chem.* **2006**, *27*, 1787−1799.

(50) Kresse, G.; Furthmüller, J. Efficient Iterative Schemes for Ab Initio Total-energy Calculations Using a Plane-wave Basis Set. *Phys. Rev. B: Condens. Matter Mater. Phys.* **1996**, *54*, 11169−11186.

(51) Blöchl, P. E. Projector Augmented-Wave Method. *Phys. Rev. B: Condens. Matter Mater. Phys.* **1994**, *50*, 17953−17979.

(52) Perdew, J. P.; Burke, K.; Ernzerhof, M. Generalized Gradient Approximation Made Simple. *Phys. Rev. Lett.* **1996**, *77*, 3865−3868.

(53) Soler, J. M.; Artacho, E.; Gale, J. D.; Garcia, A.; Junquera, J.; Ordejon, P.; Sanchez-Portal, D. The SIESTA Method for Ab Initio Order-N Materials Simulation. *J. Phys.: Condens. Matter* **2002**, *14*, 2745−2779.

(54) Troullier, N.; Martins, J. L. Efficient Pseudopotentials for Plane-Wave Calculations. *Phys. Rev. B: Condens. Matter Mater. Phys.* **1991**, *43*, 1993−2006.